

Neural networks technique based signal-from-background separation and design optimization for a W/quartz fiber calorimeter

G. Mavromanolakis *

*University of Athens, Physics Department
Nuclear and Particle Physics Division
Panepistimioupoli Ilisia, 15771, Athens, Greece*

We present a signal-from-background separation study based on neural networks technique applied to a W/quartz fiber calorimeter. Performance results in terms of signal efficiency and improvement of the signal-to-background ratio are presented. We conclude that by using neural networks we can efficiently separate signal from background and achieve a signal enhancement over the background of the order of several thousands at high efficiency.

1 Introduction

Neural networks are widely used in scientific and commercial applications due to their generally better performance compared to traditional statistical approaches and their relatively simple operation principle. In high energy physics domain they are commonly used in various pattern recognition problems e.g. for quark and gluon jet identification [1, 2, 3] or in top quark [4] and Higgs boson searches [5, 6], track finding [7, 8, 9], triggering [10]-[15], data mining, and general classification tasks. (Introduction to neural networks and review of their applications can be found in [16]-[19].)

In this paper we present a signal-from-background separation study based on neural networks technique applied to a W/quartz fiber calorimeter. The performance in terms of signal efficiency and improvement of the signal-to-background ratio, and for various calorimeter depths, read-out frequencies and total number of channels is presented.

The paper is organized as follows: in section 2 we give a general introduction on neural networks and related topics. The detector and its physics objectives are described in section 3. Section 4 contains the analysis steps and the results. We summarize and conclude in section 5.

2 Neural networks

2.1 General

A neural network (NN) is a simplified mathematical structure inspired from the real biological neural networks and their way of learning from experience, acquiring knowledge and solving problems. Their basic units are the neurons, which are interconnected through synapses and exchange signals. In general, a neuron produces an output signal which is depending on the signals it receives from the other neurons. Of great importance is the fact that the output signal is non-linearly dependent to the input, whereas the input signal is approximately the linear sum (the “coefficients” are determined by the synaptic strengths) of all the signals that are received by the neuron simultaneously. The human brain consists of $O(10^{12})$ neurons, where each neuron is

*email: gmavroma@mail.cern.ch

connected to a number, from $O(1)$ to $O(10^5)$, of other neurons. The whole structure is of immense complexity and plasticity and thus ability.

An NN has the basic concepts of a real biological neural network (neuron, connection strength, input linearity, output non-linearity) but in a much more conservative level of complexity. The neuron is a mathematical entity which has a real value depending on the connection strengths (weights) and the values of the other neurons with which it is connected. The non-linear function that relates the output from the neuron with the weights and the inputs to the neuron is usually called *activation function* and has a simple sigmoid shape bound to values in the interval $[0,1]$ or $[-1,1]$.

A neural network can be *structured* or *self-organized*. In a common structured topology the neurons are organized in layers. The *input layer*, from where the NN is fed with the input variables of the problem to be solved, followed by a number of layers, the so-called *hidden layers*, and finally the *output layer*. In the case where the information flow is in one direction only, from the input layer towards the output layer, we speak about *feed-forward* neural networks. For bidirectional connections we have *feed-back* NNs. When the output layer is fed back into the input layer then we have *recurrent networks*.

An NN is trained by a set of examples which are representative of the problem. During training the weights, which are the state variables of the network and determine its behavior, are adapted to the presented examples. In such a way the NN acquires knowledge of the rule which produced the examples and then it can generalize. Generalization means that the network can be used on real events and perform the task that was trained for. Its generalization ability is tested usually with a set of test events that we know their properties, with this procedure we validate the network's performance and afterwards it is ready to be used on real events.

The training procedure can be *supervised* or *unsupervised*. Supervised training is accomplished by presenting input-output pairs to the NN. The NN calculates its output, according to its weights, which is compared to the given desirable output. The weights are updated in such a way that the NN produces output as close as possible to the desirable one. In unsupervised training the network receives only a set of input examples without any output labeling. In this case the task is to detect some, yet unknown, structure that the real events may have.

In the following we concentrate on one of the most commonly used feed-forward neural networks, the *multilayer perceptron*. It is usually being trained with the *back-propagation algorithm* to perform event classification tasks. We describe its architecture and present the mathematical background of the training algorithm. First we discuss in brief the problem of *pattern recognition*.

2.2 Pattern recognition

Pattern recognition for event classification is a common problem encountered in high energy physics (e.g. particle identification by its shower dimension and shape, electron/hadron discrimination, trigger signal generation, quark and gluon jet classification etc.). In all cases, the problem consists in defining a procedure that should be followed in online or offline analysis, and will be able to recognize events and categorize them based on their features. A feature or pattern, is the set of properties that a class of events is characterized of, and with which this class can be possibly discriminated by the other ones. The difficulty is to reveal characteristic patterns from the measured quantities. Therefore the whole procedure is to find and properly use quantities or combination of them, that will allow correct event classification. In an approach without NNs, one usually tries to perform classification by imposing a set of one-dimensional cuts on various selected measured variables, that may characterize the events of interest. Such cuts are usually determined by examining single variable probability distributions for the events of interest and for the others (see e.g. [20]). When the complexity of the problem is increasing, better results can be obtained by employing methods that could simultaneously exploit correlations among variables.

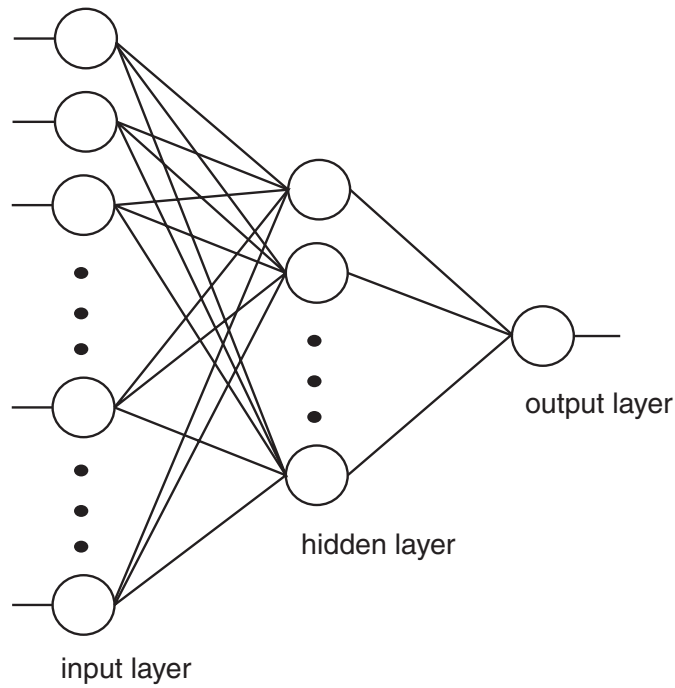


Figure 1: a multilayer perceptron with one hidden layer.

In this case a procedure with high degree of parallelism is required. The neural networks are built by concept with this kind of parallelism (neurons), and therefore they are usually used on pattern recognition tasks with outstanding performance.

2.3 Multilayer perceptron

One of the most widely used NNs for pattern recognition tasks is the multilayer perceptron. It is a feed-forward network with its neurons arranged in input, hidden and output layers (fig. 1). Every neuron is connected to all neurons of the preceding layer and of the next one, whereas there is no connection between neurons belonging to the same layer. Every neuron receives inputs from all neurons of the preceding layer, and sends its output to all ones in the next layer. All neurons obey to this connectivity scheme. Every connection is associated to a weight parameter that will be optimized during the training phase. The neuron's output is given by the activation function $f(x)$, a sigmoid function like eq. 3, that has values bound to the interval $[-1, 1]$, or like eq. 4, with values bound to the interval $[0, 1]$. The parameter T , usually called temperature of the network, determines how steep the sigmoid function is, the lower T the steeper sigmoid. In general the final performance does not depend on T , a value equals to 1 is the usual choice. The input layer consists of a number of neurons which is equal to the N_{input} input variables that will be used for the event classification.

Presenting these in mathematical form, we define I_i^k to be the input to the i th neuron in the k th layer, which consists of N^k (*) neurons, O_i^k to be the output of the i th neuron in the k th layer and w_{ji}^{k-1} to be the weight of the connection between the j th neuron in the $(k-1)$ th layer and the i th neuron in the k th layer. Then :

$$I_i^k = \sum_{j=1}^{N^{k-1}} w_{ji}^{k-1} O_j^{k-1} \quad , \quad k > 1 \quad (1)$$

$$O_i^k = f(I_i^k + w_{i0}^k) \quad , \quad k > 1 \quad (2)$$

*in this notation k serves as an index and not as an exponent value

where $f(x) \equiv$ sigmoid function, e.g.

$$f(x) = \tanh(x/T) \quad (3)$$

or

$$f(x) = \frac{1}{1 + e^{-x/T}} \quad , \quad (4)$$

and w_{i0}^k is a so-called *bias* or *threshold* of the neuron. During the training phase it is simply considered as a weight and it is optimized in a same way.

For $k = 1$ (input layer) it is :

$$O_i^1 \equiv I_i^1 = \text{input variables} \quad , \quad i = 1, \dots, N_{input} \quad (5)$$

The output layer may consist of one neuron and in this case the network is suitable for two classes separation problem. In general there may be N_{output} neurons when the events should be categorized in $2^{N_{output}}$ classes. In this case the k th bit in a binary representation of the class number is determined by the value of the k th output neuron. Alternatively, the individual N_{output} neurons could be associated with particular classes among of N_{output} possible choices.

Concerning the number of hidden layers, a general rule is that no more than two hidden layers should be needed [16]. Experience shows that whether a multilayer perceptron with two hidden layers performs satisfactorily or not, then by adding to it more hidden layers its performance is not improved. In most cases only one hidden layer is sufficient. In fact for problems of function approximation, it has been shown [21, 22, 23] that a linear combination of sigmoids can approximate any continuous function of one variable or more. Obviously (eq. 1, 2) this can be achieved with a network with one hidden layer.

Concerning the number of hidden neurons that a NN should have, there is no general rule that could suggest which number is optimal. In general the number of hidden neurons should be large enough to ensure a high degree of classification, and small enough to ensure a high degree of generalization. If there are too many hidden neurons, the network tends to learn to recognize only the set of examples that were used for its training. Therefore its generalization ability is poor and it does not perform well on a test sample or/and on real events. If the number of neurons is too small, the network performs bad since during the training phase it is unable to learn to classify.

In the following we describe the back-propagation algorithm which is usually used for training a multilayer perceptron.

2.4 Back-propagation algorithm

The back-propagation algorithm is a supervised training method often used with various modifications for training feed-forward networks. A set of examples is presented to the network which determines its output according to its state variables, the weights. The output is compared to the desired target output that each example is labeled with. By the difference between the network's output and the target one, a so-called *error* or *cost function* is determined. It is actually a function of the weights, and the algorithm should update and modify these free parameters in such way that the error function is minimized, or in other words the network's output is as close as possible to the target output. The minimization is done with a gradient descent method with respect to the weights.

We describe the algorithm following the notation given in the previous subsection. We consider a multilayer perceptron that is composed of $H + 2$ layers (an input layer, H hidden ones and

an output layer). There are $N_{weights}$ parameters (connection weights and thresholds are simply called weights) that should be optimized, where

$$N_{weights} = \sum_{k=2}^{H+2} (N^k + N^k N^{k-1}) \quad (6)$$

The error function is defined as

$$E(t) = \frac{1}{2} \sum_{n=1}^{N_{examples}} (O(n; t) - T(n))^2 \quad (7)$$

where $O(n; t)$ is the output of the network corresponding to the n th example after the minimization process has been iterated t times, and $T(n)$ is the target output associated with the example. For simplicity we consider the case of event classification between two classes (signal associated with target output $T = 1$ and background with $T = 0$), and so the output layer has only one neuron (denoted as O^{H+2} or simply O).

The weights are modified after each iteration according to

$$w_{ji}^k(t+1) = w_{ji}^k(t) + \Delta w_{ji}^k(t+1) \quad , \quad k = 1, \dots, H+1 \quad (8)$$

with

$$\Delta w_{ji}^k(t+1) = -\eta \frac{\partial E(t)}{\partial w_{ji}^k(t)} + \alpha \Delta w_{ji}^k(t) \quad , \quad k = 1, \dots, H+1 \quad (9)$$

where the parameter η (*learning factor*) determines the step of change, and thus the training rate, and α (*momentum coefficient*) is a smoothing parameter that helps the method to avoid getting stuck around the local minima of the error function.

The partial derivative of the error function is given by the recurrent relations (event and iteration indices are not shown for convenience)

$$\frac{\partial E}{\partial w_{ji}^k} = D_i^{k+1} \cdot \left. \frac{\partial f(x)}{\partial x} \right|_{x=I_i^{k+1} + w_{i0}^{k+1}} \cdot O_j^k \quad , \quad k = 1, \dots, H+1 \quad (10)$$

with

$$D_i^{k+1} = \sum_{l=1}^{N^{k+2}} D_l^{k+2} \cdot \left. \frac{\partial f(x)}{\partial x} \right|_{x=I_l^{k+2} + w_{i0}^{k+2}} \cdot w_{il}^{k+1} \quad , \quad k = 1, \dots, H \quad (11)$$

and

$$D^{H+2} = O^{H+2} - T \quad (12)$$

As can be seen in equations 10 and 11, the update information flows back from the last layer to the previous one (back-propagated). The weights of the neural network can be updated either after each example presentation (*online training*), or after the whole set of examples has been processed (*batch training*).

In general, we anticipate to reach a state in which the update differences Δw_{ji}^k are zero or close enough to it. After the training phase, we validate the quality of classification task that the network achieved with a test sample of events (generalization ability). The neural network is now ready to classify real events, that has never seen before, with known classification efficiency.

The main disadvantage of the algorithm presented above, often called as the *standard back-propagation method*, is that it converges very slowly to the minimum of the error function. Besides this convergence time grows very fast with the complexity of the problem and the size of the network. There are a couple of decades of different methods, that are based on the core features of the standard one, which achieve to speed up the overall performance significantly, at least in most cases, by e.g. defining a different error function, changing the learning factor or the network's temperature with iteration, using second order derivatives or adding extra terms, or even by allowing the network to generate or destroy neurons (self-generation) in order to reach better performance. For a rigorous description and references on several methods consult [16].

For any training method, concerning the number of example events ($N_{examples}$) that one should use on training, a general rule is that it should be one or two orders of magnitude larger than the number of weights ($N_{weights}$) which are composing the neural network. This is imposed by the fact that the generalization ability depends mainly on the ratio $N_{weights}/N_{examples}$. Actually, for a multilayer perceptron with one hidden layer it has been shown that the generalization error is of $O(N_{weights}/N_{examples})$ [24].

Of special care is the question on when the training phase should be stopped. The answer to this is, whenever there is indication of network *over-training*. This is the case where the network starts learning to recognize only the set of training examples, and as a consequence, losing its generalization ability. This can be avoided by performing training and testing in parallel and inspect the evolution of the error function for both samples with respect to the iteration of the training algorithm. When the value of the error function on the testing examples starts to increase, while on the training ones it continues decreasing, there is danger of over-training if we continue the training procedure. There is no rule that associates maximum number of iterations with over-training or with best training. Generally, this depends on the complexity of the classification problem, the complexity of the neural network, the training method and its learning factor. If a network does not show satisfactory performance before over-training occurs, then it means that the approach to that classification problem with neural network technique unfortunately fails.

We close this introduction to neural networks by adding another, somehow abstract but at the same time hopefully more clear, description of the neural networks approach to pattern recognition problems. The whole procedure can be considered as a fitting problem of $N_{examples}$ "points" on an $N_{input} \times N_{output}$ -dimensional "plane" with a "curve" (neural network) of $N_{weights}$ free parameters. The best fitting "curve" (trained neural network), is simply represented by a function parameterized by the weights (free parameters that were optimized) that receives N_{input} arguments (the network's input variables) and returns a value (results in the output layer) which approximates the corresponding "point's position" (classification).

3 The CASTOR calorimeter

3.1 Motivation

Cosmic rays experiments have detected events with unusual properties, the so-called *Centauro* events [25]-[30], which exhibit small particle multiplicity compared to normal hadronic events, complete absence or strong suppression of the electromagnetic component ($N_{hadrons}/N_{\gamma} \gg 1$, $E_{hadrons}/E_{\gamma} \gg 1$) and very high $\langle p_t \rangle$. Furthermore, a number of hadron-rich events are accompanied by a strongly penetrating component observed in the form of halo [26], strongly penetrating clusters [27] or long-living cascades, whose transition curves exhibit a characteristic form with many maxima and slow attenuation (e.g. fig. 3) [30, 31]. These events can not be explained in terms of statistical deviation from conventional hadronic physics [32, 33, 34].

According to a phenomenological model [35, 36, 37], the Centauros are considered to be the

products of hadronization of a deconfined quark-matter fireball formed in nucleus-nucleus collisions in the upper atmosphere. The “long penetrating objects” usually accompanying them are assumed to be long-lived strangelets, that may have been formed because of a mechanism of strangeness separation [39, 38] of the fireball’s strange quark content and are emitted during fireball’s hadronization. In a similar way, this kind of events and particles may be produced in Pb+Pb collisions at the LHC ($\sqrt{S} = 5.5$ TeV/nucleon) from the hadronization of a Quark Gluon Plasma state formed in the beam fragmentation region.

3.2 Detector description

The CASTOR detector [40, 41] is a Cherenkov effect based sampling calorimeter with a tungsten absorber and quartz fibers as active material. The signal is the Cherenkov light produced by the shower charged particles traversing the fibers. The calorimeter is azimuthally divided in 8 octants and longitudinally segmented in layers. Each absorber layer is followed by a number of quartz-fiber planes, altogether consisting a W-fiber layer. The W-fiber layers have 45° inclination with respect to the beam axis to achieve maximum light production. The calorimeter consists of several channels per octant. One channel consists of a number of consecutive W-fiber layers, the signal of which is collected and transmitted to its corresponding photomultiplier through an air-core lightguide (fig. 2). The calorimeter is proposed as a very forward detector of the ALICE [42] or CMS [43] experiments at the LHC covering the pseudorapidity range $5.46 \leq \eta \leq 7.14$. Its main objective is to search in the baryon rich, very forward rapidity region of central Pb+Pb collisions for unusual events and “long penetrating objects”, assumed to be strangelets, by measuring the hadronic and electromagnetic energies and the hadronic shower’s longitudinal profile on an event-by-event mode.

Detailed simulation studies of the performance of the CASTOR calorimeter have been done [44, 45]. The calorimeter shows linear response to electrons and hadrons, satisfactory energy resolution and very narrow visible transverse size of electromagnetic and hadronic showers, a property that derives from the detector’s operation principle, based on the Cherenkov effect, which makes such calorimeters sensitive essentially only to the shower core [46, 47]. Concerning the lightguides, their shape, dimensions and inner walls have been studied [48] and are optimized for better light transmission efficiency.

In this point we wish to refer the ALICE-PMD (Photon Multiplicity Detector) [49], which covers the pseudorapidity region $1.8 \leq \eta \leq 2.6$ and is dedicated to the measurement of photon and charged particle multiplicities. It is designed for Centauro events related research but from a different viewpoint. Its objective is to detect possible large non-statistical fluctuations on an event-by-event basis which is the primary signature of the formation of Disoriented Chiral Condensate (e.g. [50]). Also, concerning strangelets research in the central rapidity region covered by the ALICE barrel detector, a similar search as has been performed on recent fixed target heavy-ion experiments (NA52 [51, 52] at CERN-SPS and E864 [53, 54, 55] at BNL-AGS), aiming on detection of particles with low charge-to-mass ratio, is foreseen [56, 42] using the central tracking system. (For a rigorous review on strange quark matter searches consult [57]).

3.3 “Long penetrating objects”

The hypothesis that the long penetrating objects may be strangelets is supported by simulations [58] which show that the passage of a strangelet through matter produces shower which is slowly attenuated, long penetrating and has a longitudinal profile with many maxima structure, as observed in cosmic rays experiments [30, 31]. The passage of strangelets through the CASTOR calorimeter has been also simulated [59] and the analysis of the results has shown that the signal can be easily distinguished from the hadronic background for strangelets with energy greater than 20 TeV. Nevertheless, strangelets with a such high energy are expected to be boosted in high rapidity (and thus pseudorapidity) and as a consequence it is very likely that they pass outside the

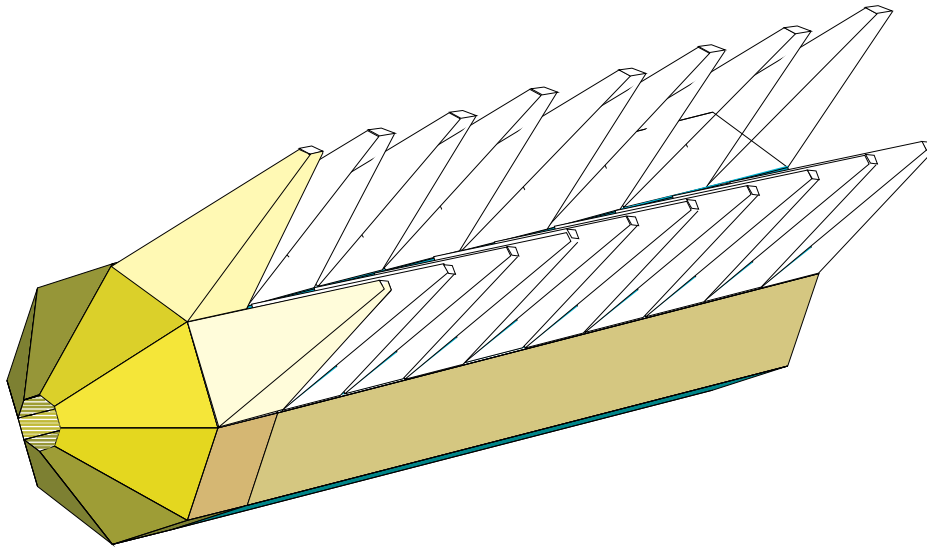


Figure 2: schematic view of the CASTOR calorimeter, some of its air-core lightguides are shown.

detector’s coverage. In addition, for the identification of lower energy strangelets, a calorimeter with very high read-out frequency is required, which is not feasible. In this study we present a sophisticated method based on neural networks technique for the separation of the low energy strangelets signal from the hadronic background.

4 Signal-from-background separation analysis

The forward region ($5.46 \leq \eta \leq 7.14$) covered by the CASTOR calorimeter receives 200 ± 11 TeV per central Pb+Pb collision at $\sqrt{S} = 5.5$ TeV/nucleon, carried by about 2000 particles (event generated by HIJING [60]). This amount of energy is associated with the conventional hadronic events, treated as background for CASTOR’s research interests. We make the basic assumption that in case that a strangelet is produced in a Pb+Pb collision, the energy not carried by it is going into conventional particle production as described by the event generator. In other words, although the detector may receive the same amount of energy, in the first case the event should be considered as not interesting (background), whereas in the second one, as signal. The only discriminating feature between them is the fact that the strangelet’s passage through the detector gives a shower with many maxima and negligible attenuation.

We study the case of a 5 TeV strangelet, an amount of energy which corresponds to 2.5% of the total energy per event that is received by the calorimeter, a fact that makes the separation task not trivial because of mainly two reasons. First, the characteristic pattern of the longitudinal development of the shower is weak and can be easily masked and suppressed by fluctuations of the showers of the other hadrons. Second, due to the fact that the calorimeter is divided in a reasonable (low) number of channels, and thus the characteristic many-maxima signal is likely to be distributed to consecutive channels and undersampled. The situation would be even worse with a detector which was not azimuthally divided. The 8 octants of the CASTOR detector are operating as stand-alone calorimeters since the visible shower transverse size is very narrow [44, 45].

We should also mention the fact that we must be able to cope with an expected signal-to-background ratio (in the raw data recorded) of the order of $1/10000$. As it is shown in the followings, by using neural networks we can surpass these difficulties and achieve very efficient separation of signal from background.

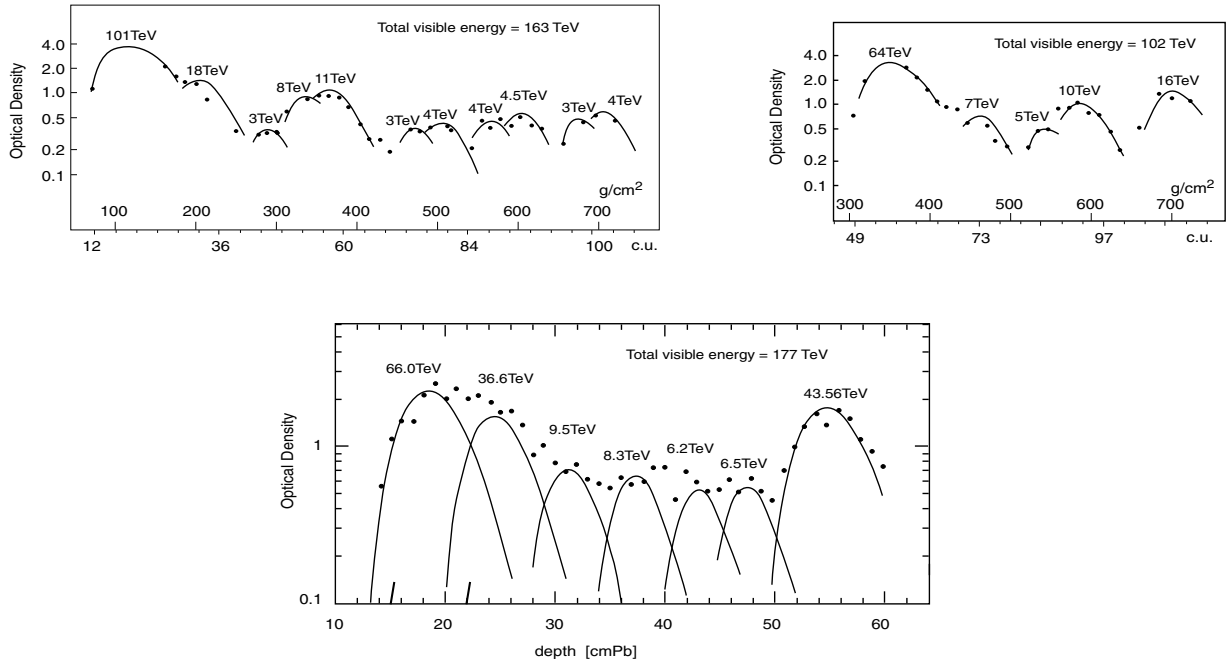


Figure 3: longitudinal profile of “long penetrating objects” observed in multilayer lead-emulsion chambers (top two plots from [31], bottom one from [30]).

4.1 Analysis steps description

Since the calorimeter is composed of 8 octants which are operating and read-out as individual detectors, the task of event classification consists in disentangling an octant which contains the signals of a strangelet and the accompanying particles (signal event) from an octant which contains only conventional signal (background event). The neural network is fed with input variables that are the responses of the channels of the octant and should provide a discriminating value (NNoutput) which is close to 1 for signal events and 0 for background ones. A typical distribution of signal and background events as a function of NNoutput is shown in fig. 4. By applying a suitable cut ($NNoutput_{cut}$) we can select a subset which contains sufficiently high number of signal events and low number of contaminating background. We define the followings:

signal efficiency, ϵ_s , which represents the probability of classification of a real signal event as signal,

$$\text{signal efficiency: } \epsilon_s = \frac{N_{signalNN}}{N_{signal}} \quad (13)$$

where $N_{signalNN}$ is the number of events that have been selected out of N_{signal} signal events due to the fact that they produce a NNoutput which satisfies the condition to be greater than the imposed cut value $NNoutput_{cut}$,

contamination, ϵ_b , which represents the probability of misclassification of a background event as signal,

$$\text{contamination: } \epsilon_b = \frac{N_{signallikeNN}}{N_{background}} \quad (14)$$

where $N_{signallikeNN}$ is the number of events that, although they belong to the set of the $N_{background}$ background events, they produce a NNoutput value which is greater than $NNoutput_{cut}$ and thus they are misclassified as signal events,

signal enhancement, $\frac{\epsilon_s}{\epsilon_b}$, which represents the factor of improvement of the signal-to-background

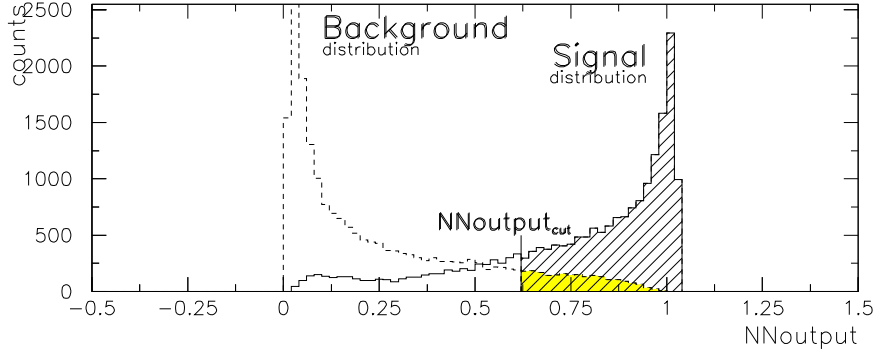


Figure 4: typical signal and background distribution as a function of NNoutput. The hatched area contains the $N_{signalNN}$ signal events that are above the selection cut $NNoutput_{cut}$. The colored area contains the contaminating $N_{signallikeNN}$ background events.

ratio,

$$signal\ enhancement = \frac{\epsilon_s}{\epsilon_b} \quad (15)$$

The parameters ϵ_s , ϵ_b , $\frac{\epsilon_s}{\epsilon_b}$ are determined at the training and testing phase of the network and quantify its performance. Then by applying the trained network on e.g. a set of raw data that was taken during experiment run and is assumed to have a signal-to-background ratio $S/B = \frac{N_{signal}}{N_{background}}$, we can result in a subset of data to be further analyzed with a signal-to-background ratio $(S/B)_{NN}$ enhanced by a factor of $\frac{\epsilon_s}{\epsilon_b}$,

$$(S/B)_{NN} = \frac{N_{signalNN}}{N_{signallikeNN}} = \frac{\epsilon_s}{\epsilon_b} \cdot \frac{N_{signal}}{N_{background}} = \frac{\epsilon_s}{\epsilon_b} \cdot S/B \quad (16)$$

For the construction of the neural networks, their training and testing we used the environment provided by the MLPfit package [61], a tool with great functionality in development of multilayer perceptrons. Other packages usually used are Jetnet [63], SNNS [64], NNO [65]. A set of 10000 signal events and 10000 background ones, which represents the calorimeter's octant simulated response to the interesting and non-interesting events as described above, is used for training the networks. A second independent set composed by 10000+10000 events is used in the testing phase. Several network architectures have been used with one hidden layer since by adding a second layer the performance is not improved. Several training algorithms have been initially used, and as expected without causing any significant change in the final network performance. We chose to work with the BFGS algorithm (Broyden-Fletcher-Godfarb-Shanno) since it is fast, very efficient and reliable [61, 62].

The general specifications of the calorimeter we used in this study are tabulated in table 1. In order to investigate how the total calorimeter depth and the total number of channels influence the signal detection efficiency, we studied 9 different configurations tabulated in table 2. They can be categorized in three cases, according to total calorimeter depth or according to depth per channel. In the following subsections we use the second categorization scheme. The results are presented in terms of signal enhancement ($\frac{\epsilon_s}{\epsilon_b}$) and signal classification efficiency (ϵ_s).

4.2 Calorimeter of 1.05 λ_I per channel

We first consider the case where each channel consists of 15 consecutive W-fiber layers, which

Table 1: calorimeter specifications.

absorber:	W ($\lambda_I=10.0$ cm, $X_0=0.365$ cm, density=18.5 gr/cm ³) maximum 170 layers, 0.5 cm thick each (= 0.071 λ_I after 45° inclination)
fiber:	quartz core (diameter 600 μm), hard plastic cladding (diameter 630 μm) numerical aperture = 0.37 3 fiber planes per absorber layer (\equiv 1 W-fiber layer)
filling ratio:	$\frac{\text{fiber volume}}{\text{absorber volume}}$: 26.5%
channels:	configurations with 7, 10, 15 consecutive W-fiber layers per channel

Table 2: calorimeter configurations.

λ_I 's(layers) per channel	# of channels(layers) per octant for calorimeter depth		
	$\sim 9.3\lambda_I$'s	$\sim 10.5\lambda_I$'s	$\sim 11.7\lambda_I$'s
0.49 (7)	19 (133)	21 (147)	24 (168)
0.70 (10)	13 (130)	15 (150)	17 (170)
1.05 (15)	9 (135)	10 (150)	11 (165)

correspond to 1.05 λ_I per channel (= 28.8 X_0 /channel). We studied calorimeters that are composed of 9, 10 and 11 channels per octant (total depth is 9.45, 10.50, 11.55 λ_I 's, respectively). Neural networks with various numbers of hidden neurons have been used. Their performances in terms of signal enhancement ($\frac{\epsilon_s}{\epsilon_b}$) as a function of signal classification efficiency (ϵ_s) are depicted in figures 5, 6 and 7. Although the performance varies among different configurations, for all cases a signal enhancement higher than 1000 can be achieved at satisfactorily high efficiency. The results from each neural network configuration are presented analytically in table 3 at page 18 and discussed in subsection 4.5.

4.3 Calorimeter of 0.70 λ_I per channel

In this case each channel consists of 10 consecutive W-fiber layers, which correspond to depth of 0.70 λ_I per channel (= 19.2 X_0 /channel). The calorimeters that have been studied are composed of 13, 15 and 17 channels per octant (total depth is 9.10, 10.50, 11.90 λ_I 's, respectively). The same procedure as in the previous case has been followed, neural networks with various numbers of hidden neurons have been studied. Their performance is shown in figures 8, 9 and 10. We can still achieve high signal enhancement and efficiency. Although the channel depth of this case is reduced by 28.6% compared to the previous one, we observe that the performance is not significantly improved. The results from each neural network configuration are presented analytically in table 3 at page 18 and discussed in subsection 4.5.

4.4 Calorimeter of 0.49 λ_I per channel

We studied also the case where each channel consists of 7 consecutive W-fiber layers, corresponding to depth of 0.49 λ_I per channel (= 13.4 X_0 /channel). Calorimeters of total depth 9.31, 10.29 and 11.76 λ_I 's have been studied (composed of 19, 21 and 24 channels per octant, respectively). A significantly improved performance should be reached to justify the high cost, due to large number

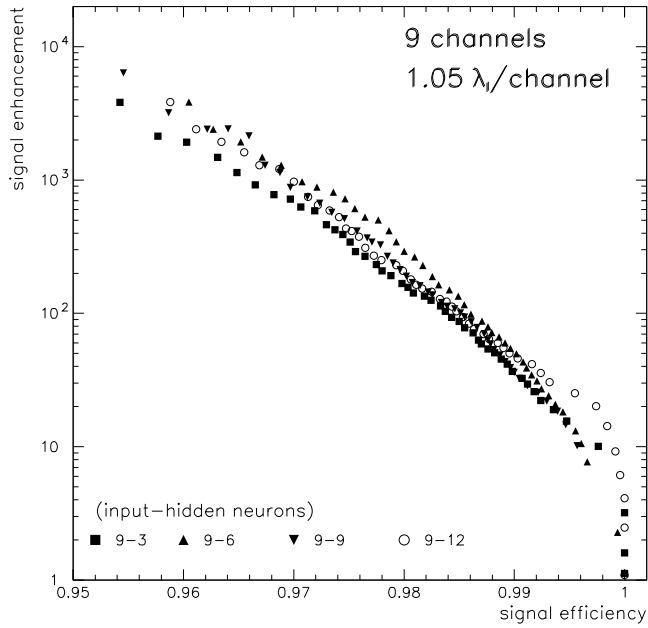


Figure 5: signal enhancement ($\frac{\epsilon_s}{\epsilon_b}$) as a function of signal efficiency (ϵ_s) for a calorimeter with 9 channels/octant and total depth of 9.45 λ_I 's.

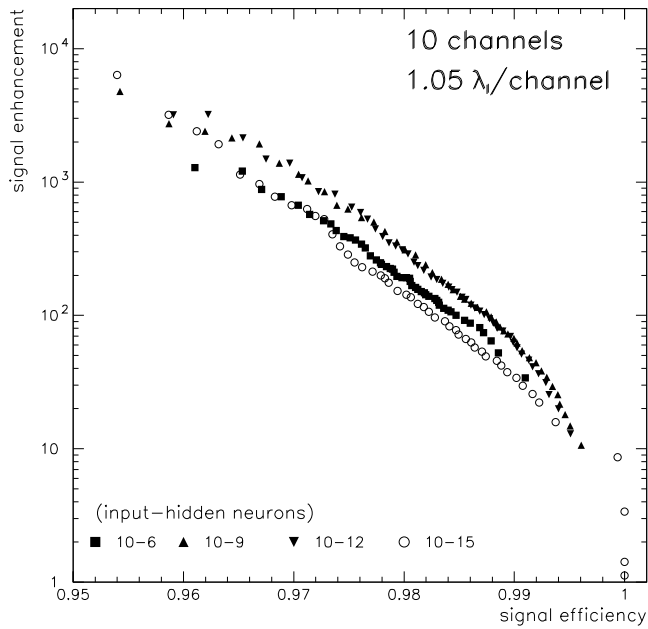


Figure 6: signal enhancement ($\frac{\epsilon_s}{\epsilon_b}$) as a function of signal efficiency (ϵ_s) for a calorimeter with 10 channels/octant and total depth of 10.50 λ_I 's.

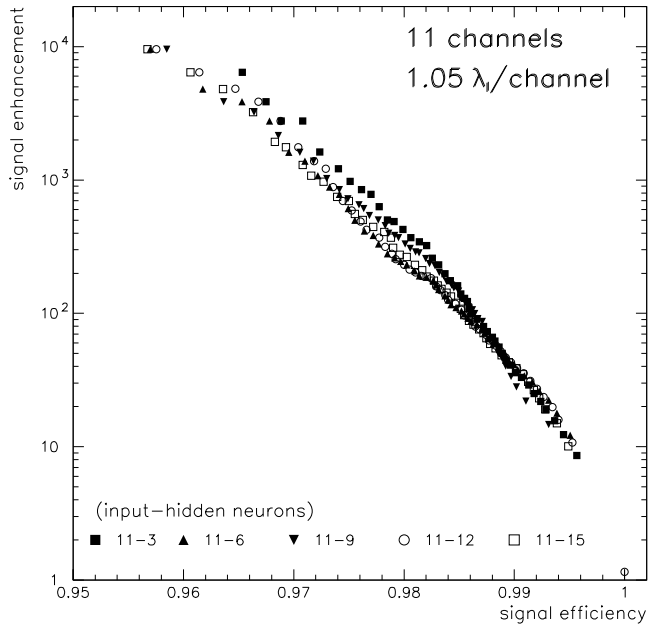


Figure 7: signal enhancement ($\frac{\epsilon_s}{\epsilon_b}$) as a function of signal efficiency (ϵ_s) for a calorimeter with 11 channels/octant and total depth of 11.55 λ_I 's.

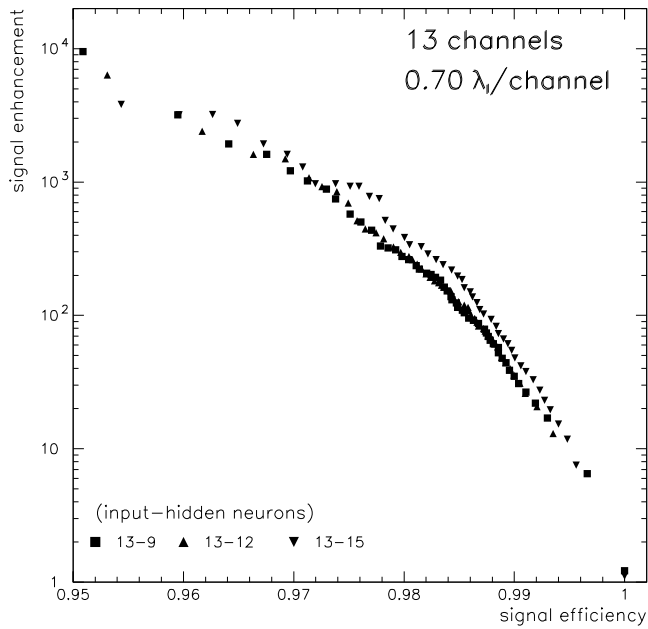


Figure 8: signal enhancement ($\frac{\epsilon_s}{\epsilon_b}$) as a function of signal efficiency (ϵ_s) for a calorimeter with 13 channels/octant and total depth of 9.10 λ_I 's.

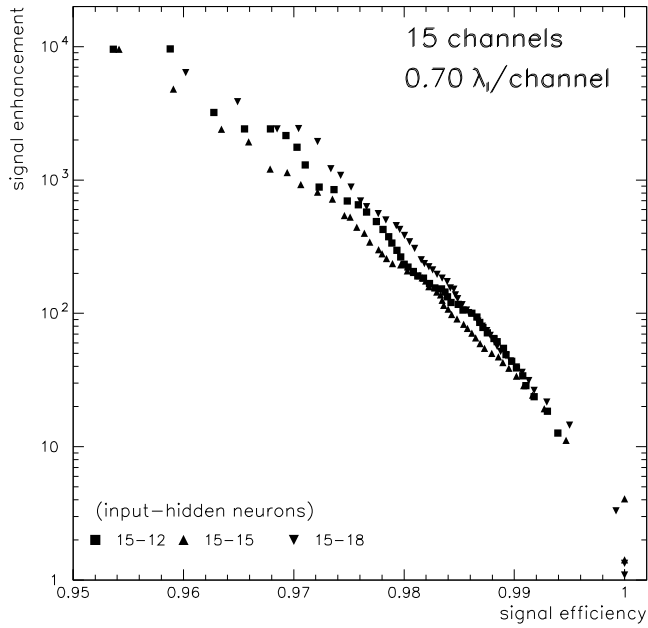


Figure 9: signal enhancement ($\frac{\epsilon_s}{\epsilon_b}$) as a function of signal efficiency (ϵ_s) for a calorimeter with 15 channels/octant and total depth of $10.50 \lambda_I$'s.

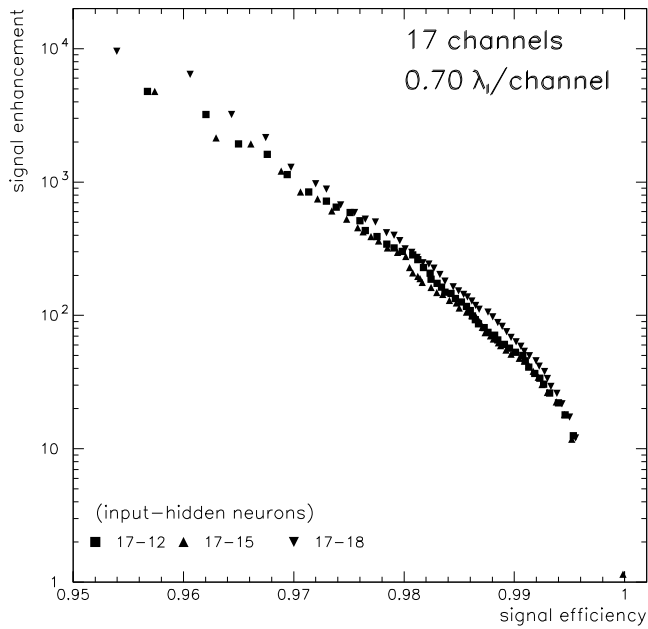


Figure 10: signal enhancement ($\frac{\epsilon_s}{\epsilon_b}$) as a function of signal efficiency (ϵ_s) for a calorimeter with 17 channels/octant and total depth of $11.90 \lambda_I$'s.

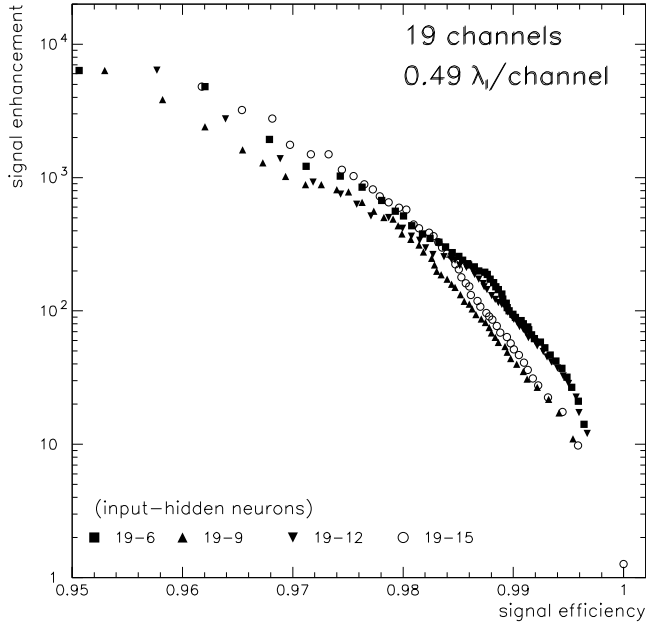


Figure 11: signal enhancement ($\frac{\epsilon_s}{\epsilon_b}$) as a function of signal efficiency (ϵ_s) for a calorimeter with 19 channels/octant and total depth of $9.31 \lambda_I$'s.

of channels. We followed the same procedure as in the previous cases. The performance of the neural networks that have been used is depicted in figures 11, 12 and 13. The signal enhancement $\frac{\epsilon_s}{\epsilon_b}$ at fixed efficiency $\epsilon_s = 0.96$ and the efficiency ϵ_s at fixed $\frac{\epsilon_s}{\epsilon_b} = 1000$ are presented for each NN architecture in table 3 at page 18. In general, although the performance in terms of achievable signal enhancement and efficiency is very satisfactory, it is not considerably better compared to that of 1.05 or $0.70 \lambda_I$ /channel cases.

In the following we discuss the results of the various calorimeter configurations and neural network architectures that have been studied.

4.5 Results recapitulation

The signal enhancement $\frac{\epsilon_s}{\epsilon_b}$ at $\epsilon_s = 0.96$ and the signal classification efficiency ϵ_s at $\frac{\epsilon_s}{\epsilon_b} = 1000$ are presented for each neural network architecture and calorimeter configuration in table 3. As proposed in [66, 19] we average the performance of the different neural networks which correspond to the same calorimeter configuration. The results are tabulated in table 4 and plotted in figures 14 and 15 (points are grouped according to depth per channel and total calorimeter depth, respectively). We observe that the signal enhancement is increasing by increasing calorimeter depth and/or decreasing depth per channel. The signal efficiency stays basically unchanged, thus the use of a deep calorimeter with frequent read-out results in more efficient background discrimination (so lower contamination).

Generally, in all calorimeter configurations that have been studied, the signal-background classification task as performed by neural networks can provide a signal-over-background enhancement factor, $\frac{\epsilon_s}{\epsilon_b}$, larger than 2000(1000) at high signal classification efficiency, ϵ_s , of a value of 0.96(0.97). This performance is considered very satisfactory and can be achieved even with a moderately short calorimeter ($9.45 \lambda_I$'s deep) with a conservative number of channels (9 channels per octant, $1.05 \lambda_I$ /channel). In the case of very frequent read-out ($0.49 \lambda_I$ /channel), the performance in terms of achievable signal enhancement and efficiency is improved. But still is not considerably

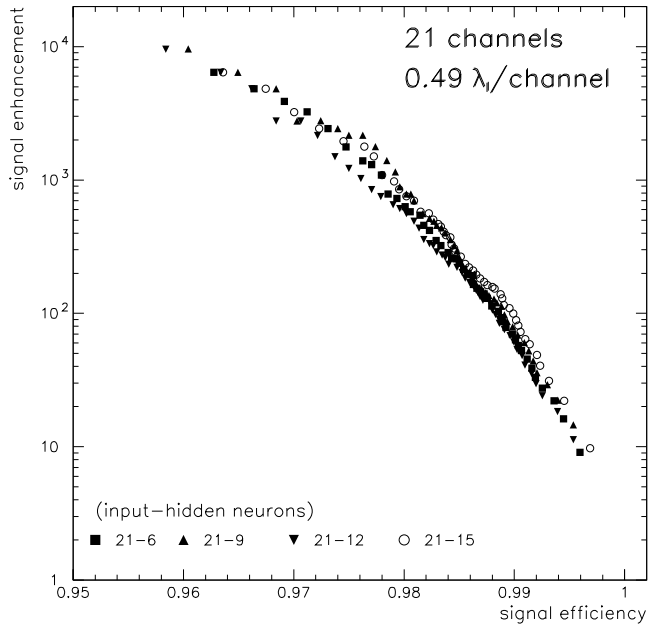


Figure 12: signal enhancement ($\frac{\epsilon_s}{\epsilon_b}$) as a function of signal efficiency (ϵ_s) for a calorimeter with 21 channels/octant and total depth of $10.29 \lambda_I$'s.

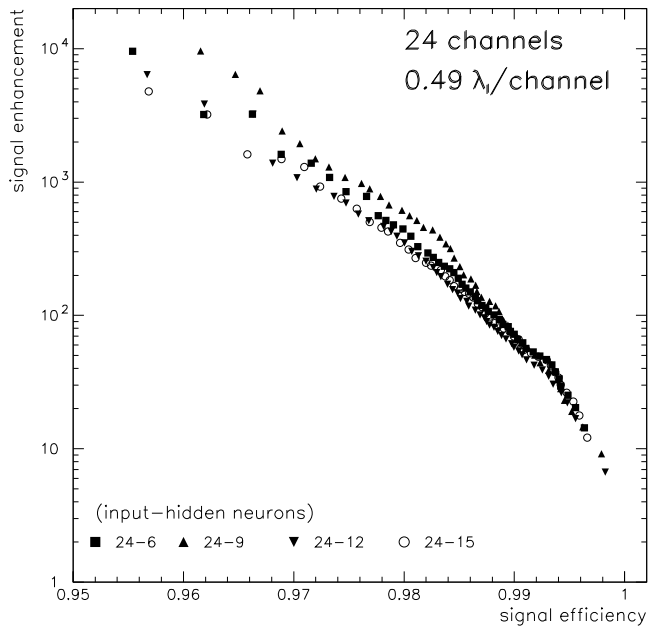


Figure 13: signal enhancement ($\frac{\epsilon_s}{\epsilon_b}$) as a function of signal efficiency (ϵ_s) for a calorimeter with 24 channels/octant and total depth of $11.76 \lambda_I$'s.

better, compared to the cases of 1.05 or 0.70 λ_I /channel read-out, to justify the higher cost of the large total number of calorimeter channels. If we had to choose a configuration out of the 9 ones that have been studied, we would suggest either the case of a calorimeter of 11.55 λ_I 's deep with 11 channels per octant (1.05 λ_I /channel) or one with depth of 10.50 λ_I 's with 15 channels per octant (0.70 λ_I /channel), since they both combine adequate number of channels and total depth with high performance and cost efficiency.

5 Summary and conclusions

We presented a signal-from-background separation study based on neural networks technique. We used a multilayer perceptron with one hidden layer that was fed with input variables that were the channel responses of each octant of the CASTOR calorimeter. The network was trained to distinguish between an octant, which contained the characteristic pattern of the longitudinal development of the shower of a “long-penetrating object” (strangelet), and an octant, which contained only signals from conventional particle showers.

We concentrated on the case of a strangelet with energy of 5 TeV, an amount which corresponds to 2.5% of the total energy per event that is expected to be received by the calorimeter. We studied calorimeter configurations with various total depths and depths per channel. The results show that we can very efficiently separate the signal from the background and compensate the initial signal-to-background ratio which is expected to be of the order of 1/10000. The neural networks based classification task can provide a signal-over-background enhancement factor larger than 2000(1000), at signal classification efficiency as high as 0.96(0.97), and thus resulting to a selected subset of events to be further analyzed with a significantly improved signal-to-background ratio of the order of 0.1 or higher. We stress the fact that this performance is achieved without any preprocessing or preselection procedure, thus an even higher signal-to-background ratio might be accomplished.

Concerning the optimum calorimeter configuration in terms of total depth and read-out frequency, we conclude that a total depth between 11.55 and 10.50 λ_I 's and with 1.05-0.70 λ_I /channel (10 to 15 channels per octant) is sufficient to ensure high classification performance. The fact that such good performance corresponds to a 5 TeV strangelet leads in concluding that similar or even better performance can be achieved for strangelets of higher energy since their signal will be stronger and more pronounced.

Table 3: signal enhancement $\frac{\epsilon_s}{\epsilon_b}$ at $\epsilon_s = 0.96$ and signal efficiency ϵ_s at $\frac{\epsilon_s}{\epsilon_b} = 1000$ for the studied configurations and neural network architectures.

calorimeter read-out	inputs (\equiv channels)	hidden neurons	$\frac{\epsilon_s}{\epsilon_b}$ at $\epsilon_s = 0.96$	ϵ_s at $\frac{\epsilon_s}{\epsilon_b} = 1000$	
1.05 λ_I /channel	9	3	1921	0.966	
		6	3842	0.971	
		9	2800	0.969	
		12	3119	0.970	
	10	6	1281	0.966	
		9	2572	0.971	
		12	3197	0.971	
		15	2799	0.967	
	11	3	6435	0.975	
		6	7190	0.973	
		9	6720	0.973	
		12	6410	0.973	
		15	6404	0.973	
	0.70 λ_I /channel	13	9	3198	0.971
			12	2404	0.972
15			3199	0.974	
15		12	6399	0.972	
		15	4796	0.970	
		18	6401	0.975	
17		12	3996	0.970	
		15	3464	0.970	
		18	4809	0.972	
0.49 λ_I /channel		19	6	5574	0.974
			9	3832	0.970
			12	4570	0.972
	15		4809	0.976	
	21	6	6418	0.978	
		9	8019	0.979	
		12	8004	0.976	
		15	6424	0.979	
	24	6	3206	0.973	
		9	9615	0.975	
		12	5113	0.970	
		15	3995	0.972	

Table 4: average signal enhancement ($\frac{\epsilon_s}{\epsilon_b}$ at $\epsilon_s = 0.96$) and average signal efficiency (ϵ_s at $\frac{\epsilon_s}{\epsilon_b} = 1000$) for the studied calorimeter configurations.

channels	$\lambda_I/\text{channel}$	depth (λ_I)	$\frac{\epsilon_s}{\epsilon_b}$ at $\epsilon_s = 0.96$	ϵ_s at $\frac{\epsilon_s}{\epsilon_b} = 1000$
9	1.05	9.45	2921 ± 796	0.969 ± 0.002
10	1.05	10.50	2462 ± 829	0.969 ± 0.003
11	1.05	11.55	6632 ± 339	0.973 ± 0.001
13	0.70	9.10	2934 ± 459	0.972 ± 0.002
15	0.70	10.50	5865 ± 926	0.972 ± 0.003
17	0.70	11.90	4090 ± 677	0.971 ± 0.001
19	0.49	9.31	4696 ± 718	0.973 ± 0.003
21	0.49	10.29	7216 ± 918	0.978 ± 0.001
24	0.49	11.76	5482 ± 2864	0.973 ± 0.002

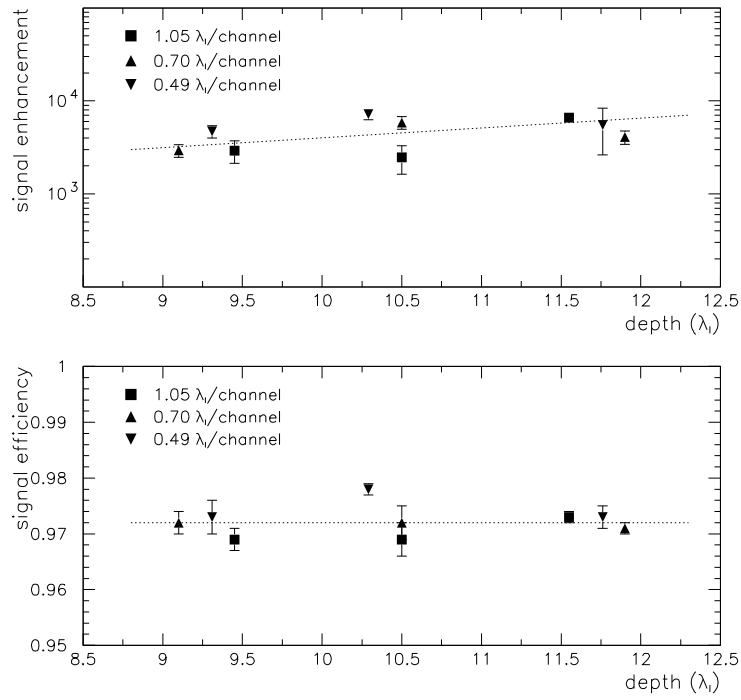


Figure 14: average signal enhancement (at $\epsilon_s = 0.96$) and efficiency (at $\frac{\epsilon_s}{\epsilon_b} = 1000$) as a function of total calorimeter depth for different channel configurations. A trendline is shown to guide the eye.

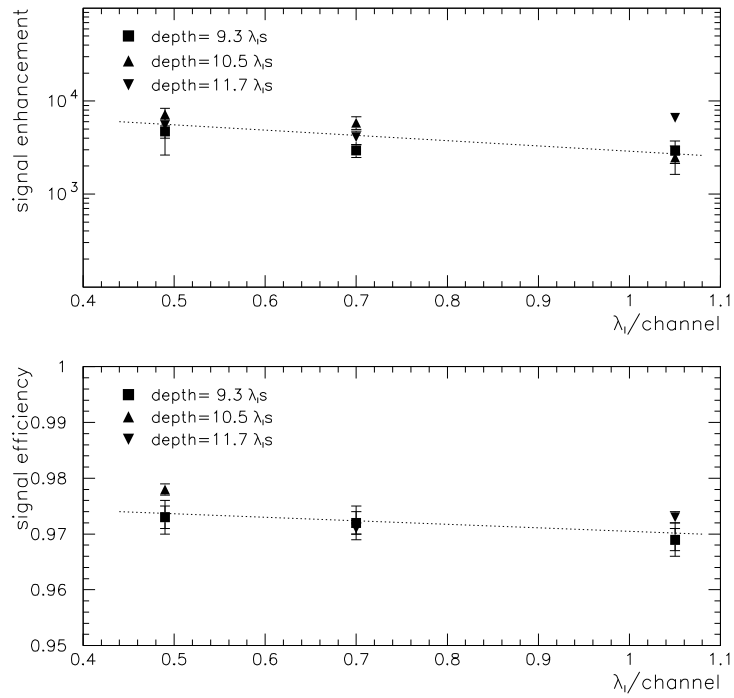


Figure 15: average signal enhancement (at $\epsilon_s = 0.96$) and efficiency (at $\frac{\epsilon_s}{\epsilon_b} = 1000$) as a function of depth per channel for different total calorimeter depths. A trendline is shown to guide the eye.

References

- [1] L.Lonnblad et al., Phys.Rev.Lett. 65(1990)1321
- [2] L.Lonnblad et al., Nucl.Phys. B349(1991)675
- [3] M.A.Graham et al., Phys.Rev. D51(1995)4789
- [4] L.Holmstrom et al., Comp.Phys.Comm. 88(1995)195
- [5] T.Maggipinto et al., Phys.Lett. B409(1997)517
- [6] K.Hultqvist et al., Nucl.Instr.Meth. A364(1995)193
- [7] B.Denby, Comp.Phys.Comm. 49(1988)429
- [8] C.Peterson, Nucl.Instr.Meth. A279(1989)537
- [9] M.Gyulassy, H.Harlander, Comp.Phys.Comm. 66(1991)31
- [10] C.S.Lindsey et al., Nucl.Instr.Meth. A317(1992)346
- [11] B.Denby et al., Nucl.Instr.Meth. A356(1995)485
- [12] F.R.Leimgruber et al., Nucl.Instr.Meth. A365(1995)198
- [13] J.H.Kohne et al., Nucl.Instr.Meth. A389(1997)128
- [14] A.Baldini et al., Nucl.Instr.Meth. A389(1997)141
- [15] P.Busson et al., Nucl.Instr.Meth. A410(1998)273
- [16] C.Peterson, Th.Rognvaldsson, An Introduction to Artificial Neural Networks, 1991 CERN School of Computing, LUTP 91-23
- [17] B.Denby, Tutorial on Neural Network Applications in High Energy Physics: a 1992 perspective, in Proc. of AIHENP 1992, La Londe les Maures, France, World Scientific 1992
- [18] B.Denby, Comp.Phys.Comm. 119(1999)219
- [19] D.Horn, Nucl.Instr.Meth. A389(1997)381
- [20] K.Fukunaga, Introduction to Statistical Pattern Recognition, Academic Press, 1990
- [21] K.Hornik et al., Neural Networks 2(1989)359
- [22] G.Cybenko, Mathematics of Control, Signals and Systems 2(1989)303
- [23] K.Hornik et al., Neural Networks 3(1990)551
- [24] E.Baum, D.Haussler, Neural Computation 1(1989)151
- [25] C.M.G.Lattes, Y.Fujimoto, S.Hasegawa, Phys.Rep. 65(1980)151
- [26] L.T.Baradzei et al. (Chacaltaya and Pamir Collaboration), Nucl.Phys. B370(1992)365
- [27] S.Hasegawa, M.Tamada, Nucl.Phys. B474(1996)225
- [28] S.L.C.Barroso et al. (Chacaltaya Emulsion Chamber Collaboration), Proc. 25th Int. Cosmic Ray Conf., Durban 1997, vol.6 p.53
- [29] A.Ohsawa, Nucl.Phys. B(Proc.Suppl.) 75A(1999)3
- [30] T.Arisawa et al. (Chacaltaya and Pamir Collaboration), Nucl.Phys. B424(1994)241
- [31] Z.Buja et al., Proc. 17th Int. Cosmic Ray Conf., Paris 1981, vol.11 p.104
- [32] M.Tamada, V.V.Kopenkin, Nucl.Phys. B494(1997)3
- [33] S.L.C.Barroso et al. (Chacaltaya Emulsion Chamber Collaboration), Nucl.Phys. B(Proc.Suppl.) 75A(1999)150
- [34] M.Tamada, Nucl.Phys. B(Proc.Suppl.) 75A(1999)156
- [35] M.N.Asprouli et al., Astrop.Phys. 2(1994)167
- [36] A.D.Panagiotou et al., Phys.Rev. D45(1992)3134
- [37] A.D.Panagiotou et al., Z.Phys. A333(1989)355
- [38] C.Greiner et al., Phys.Rev.Lett. 58(1987)1825
- [39] C.Greiner et al., Phys.Rev. D38(1988)2797
- [40] A.L.S.Angelis et al., hep-ex/9901038 and in Proc. of the XXVIII Int. Symp. on Multi-particle Dynamics, Delphi, Greece, Sept.1998, eds. N.G.Antoniou et al., World Scientific, Singapore 1999, p.134
- [41] A.L.S.Angelis et al., CASTOR proposal, ALICE note CAS/97-07

- [42] ALICE Collaboration, Technical Proposal, CERN/LHCC/95-71
- [43] CMS Collaboration, Technical Proposal, CERN/LHCC/94-38
- [44] G.Mavromanolakis et al., ALICE note CAS/2000-20
- [45] G.Mavromanolakis et al., ALICE note CAS/2000-25
- [46] J.Britz et al., RD40 Project, CERN/LHCC 95-27
- [47] P.Gorodetzky et al., Nucl.Instr.Meth. A361(1995)161
- [48] G.Mavromanolakis et al., ALICE note CAS/2000-27 and addendum
- [49] ALICE Photon Multiplicity Detector, Technical Design Report, CERN/LHCC 99-32
- [50] M.M.Aggarwal et al. (WA98 Collaboration), Nucl.Phys. A638(1998)249c
- [51] G.Appelquist et al. (NA52 Collaboration), Phys.Rev.Lett. 76(1996)3907
- [52] G.Ambrosini et al. (NA52 Collaboration), Nucl.Phys. A610(1996)306c
- [53] T.A.Armstrong et al. (E864 Collaboration), Phys.Rev.Lett. 79(1997)3612
- [54] T.A.Armstrong et al. (E864 Collaboration), Nucl.Phys. A625(1997)494
- [55] T.A.Armstrong et al. (E864 Collaboration), Phys.Rev. C59(1999)1829
- [56] J.P.Coffin, C.Kuhn, J.Phys. G23(1997)2117
- [57] R.Klingenberg, J.Phys. G25(1999)R273
- [58] E.Gladysz-Dziadus, Z.Wlodarczyk, J.Phys. G23(1997)2057
- [59] A.L.S.Angelis et al., Eur.Phys.J. direct C9(1999)1
- [60] X.N.Wang, M.Gyulassy, Phys.Rev. D44(1991)3501
M.Gyulassy, X.N.Wang, Comp.Phys.Comm. 83(1994)307
- [61] J.Schwindling, B.Mansoulie, MLPfit: a tool for Multi-Layer Perceptrons,
<http://www.cern.ch/schwind/MLPfit.html>
- [62] R.Fletcher, Practical methods of optimization, J.Wiley&Sons 2nd ed. 2000
- [63] C.Peterson et al., Jetnet 3.0, Comp.Phys.Comm. 88(1994)185 ;
L.Lonnblad et al., Jetnet 2.0, Comp.Phys.Comm. 70(1992)167
- [64] A.Zell et al., Stuttgart Neural Network Simulator, Univ. of Stuttgart IPVP report 6/95
- [65] M.Kunze, J.Steffens, Neural Network Objects, Nucl.Instr.Meth. A389(1997)12
- [66] D.H.Wolpert, Neural Networks 5(1992)241